metals

MDPI

Article

Dynamically Recrystallized Microstructures, Textures, and Tensile Properties of a Hot Worked High-Mn Steel

Pavel Dolzhenko, Marina Tikhonova, Rustam Kaibyshev and Andrey Belyakov *

Laboratory of Mechanical Properties of Nanstructured Materials and Superalloys, Belgorod State University, Belgorod 308015, Russia; dolzhenko.p@yandex.ru (P.D.); tikhonova@bsu.edu.ru (M.T.); rustam_kaibyshev@bsu.edu.ru (R.K.)

* Correspondence: belyakov@bsu.edu.ru; Tel.: +7-4722-585-457

Received: 5 December 2018; Accepted: 26 December 2018; Published: 2 January 2019

Abstract: The deformation microstructures and mechanical properties were studied in a high-Mn steel subjected to hot compression. The deformation microstructures resulted from the development of dynamic recrystallization (DRX). Two DRX mechanisms, namely discontinuous and continuous, operated during warm-to-hot working. Under the conditions of hot working when the flow stresses were below 100 MPa, a power law function was obtained between the DRX grain size and the true flow stress with a grain size exponent of −0.8 owing to the discontinuous DRX. On the other hand, the gradual change in the operating DRX mechanism from a discontinuous to continuous one upon a transition from hot to warm working, when the true flow stress increases above 100 MPa, resulted in the grain size exponent of about −0.5 in the power law between the flow stress and the DRX grain size. The DRX microstructures developed by warm-to-hot working provide a beneficial combination of mechanical properties including high ultimate tensile strength in the range of 700–900 MPa and sufficient ductility with a uniform elongation well above 50%. The strengthening of the samples with DRX microstructures was attributed to the combined effect of the grain size and dislocation strengthening resulting in a rather high grain boundary strengthening factor of 570 MPa $\mu m^{0.5}$ in the Hall-Petch-type relationship.

Keywords: high-Mn steel; hot working; dynamic recrystallization; grain growth; textures; yield strength

1. Introduction

Dynamic recrystallization (DRX) is a very interesting phenomenon, which can assist us in producing desired microstructures and, therefore, required properties in various metallic materials [1–3]. The most important advantage of DRX is that the beneficial microstructures can be obtained directly during hot working with the appropriate regimes. The general regularities of DRX like strain softening, DRX kinetics, DRX grain size, effect of initial microstructure, etc. have been fairly elaborated in numerous studies [4–11]. The DRX mechanisms responsible for the developed microstructures and their evolution kinetics depend on the properties of processed material, i.e., crystal lattice, stacking fault energy (SFE), phase composition, etc., and of the deformation conditions. DRX is particularly important for structural steels and alloys, of which mechanical properties sensitively depend on their microstructures.

Among a wide variety of advanced structural steels, high-Mn austenitic steels have been gaining specific attention [12–14]. These steels exhibit an improved combination of high strength and plasticity. Such outstanding mechanical behavior is achieved owing to a so-called twinning-induced plasticity (TWIP) effect [15]. The frequent deformation twinning resulting in pronounced strain hardening is a

consequence of low SFE, which is provided by a special chemical composition including a high amount of manganese along with carbon, aluminum, silicon, and other additives. The high-Mn TWIP steels are discussed as advanced structural materials for critical engineering applications, among which are car body elements and architectural seismic dampers that require enhanced toughness and fatigue properties. In spite of high practical importance, however, the deformation microstructures that evolve in high-Mn steels during hot working have not been investigated in sufficient detail. The influence of DRX on the mechanical properties in advanced high-Mn steels subjected to hot working deserves more careful analysis.

Austenitic steels with low SFE commonly experience discontinuous DRX under the conditions of hot working [2,5,16–18]. This DRX mechanism is forced by high dislocation density, i.e., work-hardening, and consists in the new grain nucleation by local migration of frequently serrated grain boundaries followed by the growth of the just-nucleated grains until a cessation of their growth. The latter is associated with both impingements of the growing grains and an increase in the dislocation density in the growing grains because of further deformation. Discontinuous DRX develops cyclically, including a consequence of the repetitive processes of DRX nucleation and DRX grain growth during the hot deformation. In this case, the mean DRX grain size can be related to the flow stress through a power law function with a grain size exponent of about -0.7 [2,7,17–19]. The grain refinement by means of DRX should lead to strengthening in accordance with a well-known Hall-Petch relationship. Thus, the steel semi-products with desirable mechanical properties can be produced by hot working under appropriate temperature/strain rate conditions. The aim of the present study is to clarify the DRX behavior and the tensile properties of an advanced high-Mn austenitic steel processed by hot deformation.

2. Materials and Methods

A high-Mn austenitic steel containing 0.6 C, 17.3 Mn, 1.6 Al, 0.06 Nb, 0.008 P, and 0.009 S (all in wt.%) with an original grain size of 18 μm was produced by vacuum melting followed by hot rolling at 1423 K. The cylindrical samples with a height of 16 mm and a diameter of 8 mm were compressed to a strain of 1.2 at temperatures of 1073 K to 1323 K and strain rates of 10^{-4} s^{-1} to 10^{-2} s^{-1} using an Instron 300LX testing machine. The compressed samples were immediately quenched by water jet as the deformation ceased.

The structural investigations were carried out on the compressed samples sectioned along the compression axis (CA) using a Nova Nano SEM 450 scanning electron microscope (SEM) (FEI, Hillsboro, OR, USA) equipped with an electron backscatter diffraction (EBSD) analyzer equipped with an orientation imaging microscopy (OIM) system. The microstructures were observed at mid-height at a third of the sample cross section diameter. The OIM images were obtained with a step size of 0.4 μm and then subjected to cleanup procedures, setting a minimal confidence index of 0.1. The mean grain size (D) was calculated with the OIM software TSL OIM Analysis 6 as an equivalent diameter of the DRX grains bounded by high-angle boundaries (HAB) with misorientations of $\theta \geq 15^{\circ}$.

The flat dog-bone-type specimens with a gauge length of 4 mm and a cross section of 1.0×0.5 mm^2 were used for tensile tests, which were carried out at room temperature and at an initial strain rate of 10^{-3} s^{-1} using an Instron 5882 testing machine (Illinois Tool Works Inc., Norwood, MA, USA).

3. Results

3.1. Hot Deformation Behavior

Representative true stress-strain curves for hot compressions of the studied high-Mn steel are shown in Figure 1. Following a rapid increase in the flow stress at an early deformation, the deformation behavior is characterized by a gradual strain softening and then a steady-state flow at rather large strains. Such deformation behavior with a peak stress is characteristic of discontinuous DRX, when developing DRX nuclei expand at the expense of work-hardened surroundings. Thus, the replacement of work-hardened grains by newly developed DRX grains

results in the strain softening on the flow curve [1–4]. The strain corresponding to the peak stress increases with a decrease in the temperature and/or an increase in the strain rate. Correspondingly, the steady-state deformation is achieved faster at higher temperatures and/or lower strain rates. This is indicative of DRX acceleration with an increase in the temperature and/or a decrease in the strain rate.

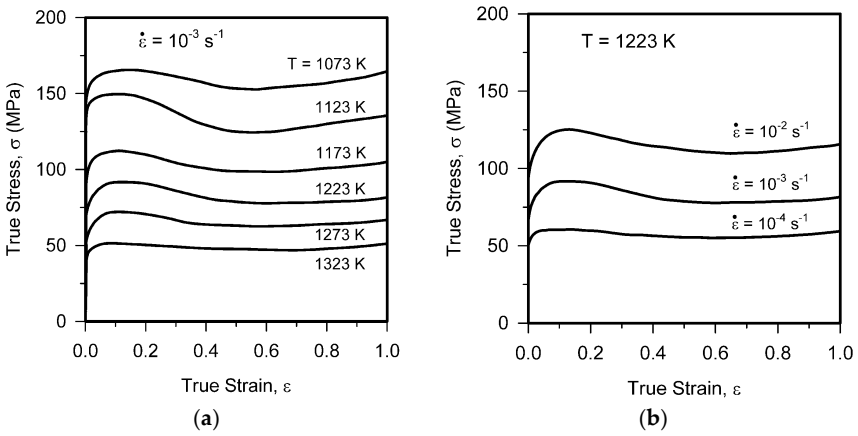

Figure 1. True stress-strain curves obtained during hot compressions of a high-Mn steel at a strain rate of 10^{-3} s^{-1} (**a**) or at a temperature of 1223 K (**b**).

The flow stresses exhibit typical hot deformation behavior. Namely, the flow stress increases as the deformation temperature decreases (Figure 1a) and/or the strain rate increases (Figure 1b). This relatively strong temperature/strain rate dependence of the flow stress is commonly discussed in terms of a power law of the temperature-compensated strain rate (Zener-Hollomon parameter), $Z = \dot{\varepsilon} \cdot \exp Q/RT$, where Q is the activation energy, R is the universal gas constant, and T is the temperature [1]. Figure 2a shows the relationship between the flow stress at steady-state deformation (σ_{ss}) and temperature (T). Four arbitrarily selected stress levels indicated by dashed lines in Figure 2a are further used in Figure 2b, which represents the relationship between the corresponding strain rates and temperatures for the chosen stress levels. It is clear from Figure 2b that all strain rates at constant steady-state stresses exhibit almost the same temperature dependencies. Therefore, the activation energy of 385 kJ/mole is obtained for the studied range of the hot working conditions. This activation energy is about 1.5 times higher than the activation energy of lattice diffusion in γ-iron of 270 kJ/mole [20]. A similar relationship between the activation energies for lattice diffusion and hot deformation has been reported in numerous other studies on the hot working of metallic materials exhibiting discontinuous DRX behavior [10,16,21–23].

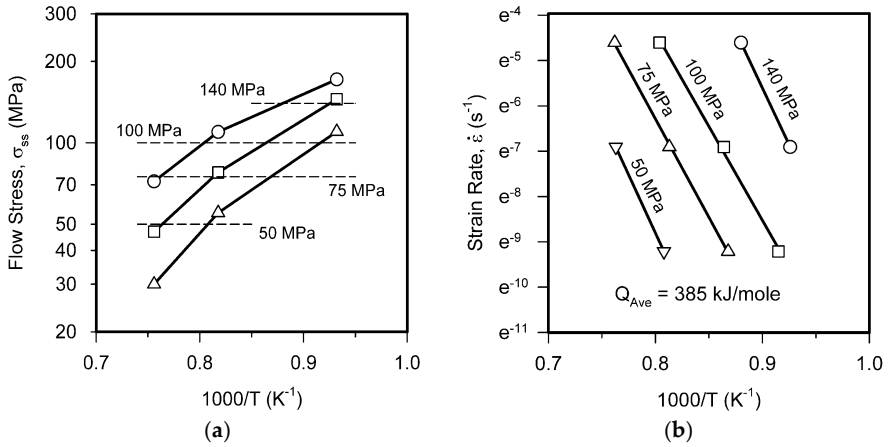

Figure 2. The temperature effect on the steady-state flow stress (**a**) or strain rate (**b**) upon hot compression of a high-Mn steel.

Figure 3 shows the relationship between the steady-state flow stress and the deformation condition expressed by the temperature-compensated strain rate, Z. The flow stress can be expressed by a power law function of Z with an exponent of 0.2 in the range of low Z in Figure 3. This agrees well with other studies on hot working and creep at elevated temperatures, when the power law relationship generally holds between the flow stress and strain rate with a stress exponent of 5 [18,20]. In contrast, the temperature and/or strain rate effect on the flow stress diminishes with an increase in Z. An exponent of about m = 0.1 is obtained for σ_{ss}—Z^m relationship in the range of high Z in Figure 2. This domain of deformation conditions corresponds to a so-called power law breakdown, when the stress exponent in the stress-strain rate relationship progressively increases with a decrease in the deformation temperature and/or an increase in the strain rate [24].

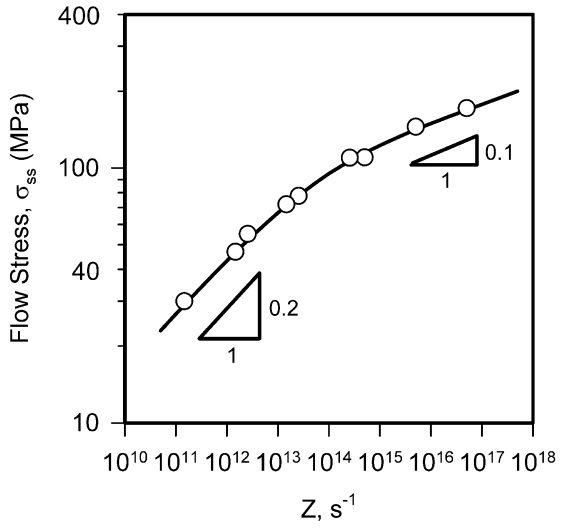

Figure 3. Steady-state flow stress vs. temperature-compensated strain rate (Z) for the hot compression of a high-Mn steel.

3.2. Microstructures and Textures after Hot Compressions

The typical microstructures developed during hot compressions at different temperatures and strain rates are shown in Figure 4. The grain size increases with a decrease in Z, i.e., an increase in the deformation temperature and/or a decrease in the strain rate. The frequently serrated grain boundaries indicate on the boundary bulging as the mechanism of DRX grain nucleation. The presence of annealing twins in the developed microstructures confirms the discontinuous DRX mechanism, which is associated with a grain boundary migration (growth of DRX nuclei) over a large distance, in the present samples, especially, after compressions under low Z conditions (Figure 4c,d). It should be noted that the sample compressed under the highest Z condition (Figure 4a) exhibits uncompleted DRX. The layers consisting of fine DRX grains locate along the grain boundaries of pan-caked large original grains, making a necklace-type microstructure. Such partially recrystallized microstructures have been frequently reported for metals and alloys subjected to warm deformation at relatively low temperatures [2,22,25].

The plot of the DRX grain size versus the steady-state flow stress is shown in Figure 5. The absolute value of the grain size exponent in the relationship between D and σ_{ss} decreases from 0.8 to 0.5 with an increase in the flow stress. Almost the same change in the grain size exponent has been observed in other austenitic steels subjected to warm deformation [2,18]. This change in the σ—D^{-N} relationship has been attributed to the change in the DRX mechanism. Namely, a relatively high grain size exponent corresponds to a discontinuous DRX under hot working conditions, whereas transition to a continuous DRX caused by a decrease in the deformation temperature to a warm working domain leads to a decrease in grain size exponent down to about 0.25 [26].

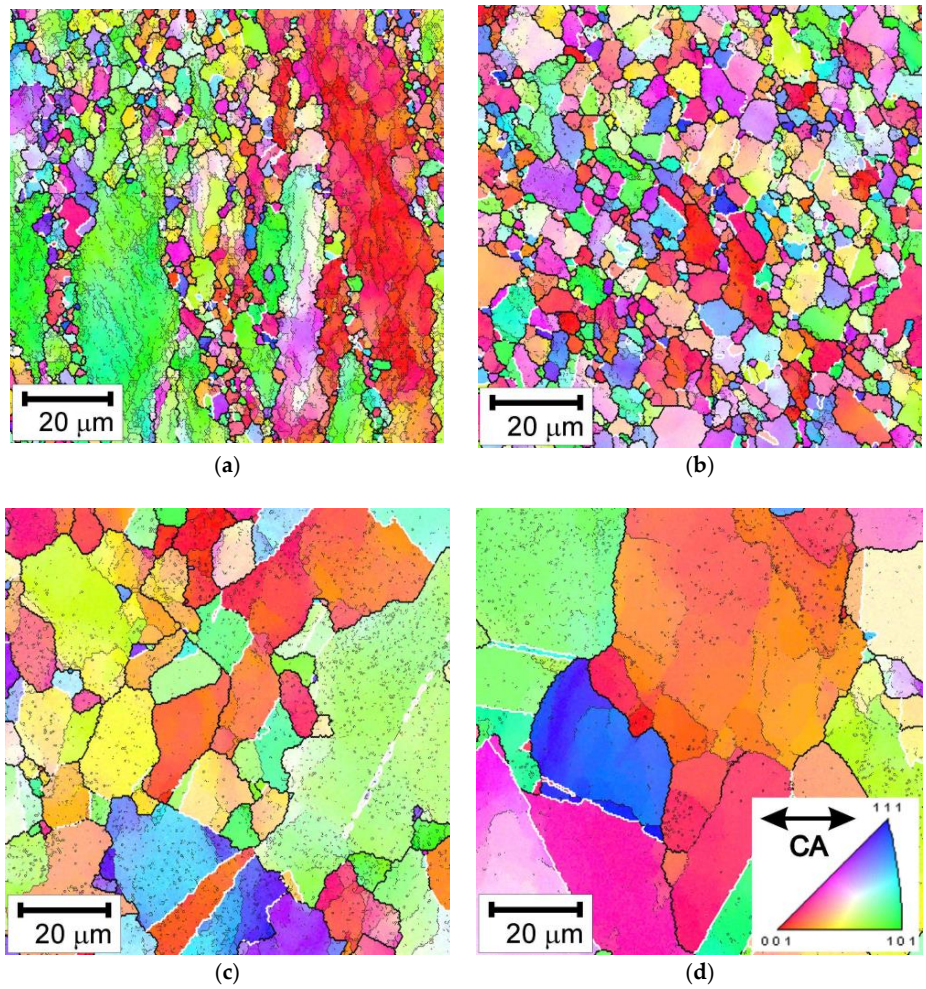

Figure 4. The typical deformation microstructures evolved in a high-Mn steel during hot compression at T = 1073 K and a strain rate of 10^{-2} s^{-1} (**a**); at 1073 K and 10^{-3} s^{-1} (**b**); at 1223 K and 10^{-3} s^{-1} (**c**); and at 1323 K and 10^{-3} s^{-1} (**d**). The colors indicate the orientation along the compression axis (CA). The high-angle boundaries, low-angle sub-boundaries, and twin boundaries are shown by the thick black lines, thin black lines, and white lines, respectively.

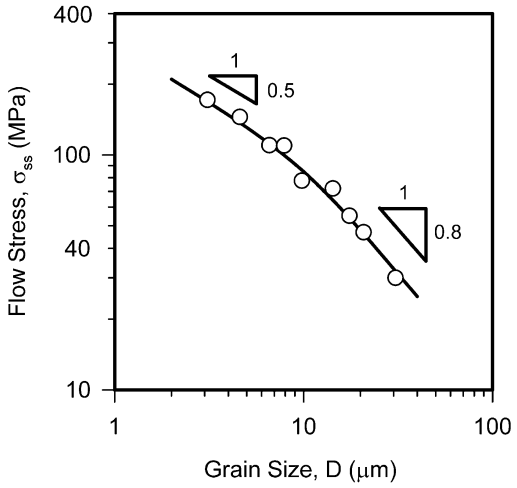

Figure 5. The relationship between the steady-state flow stress and dynamically recrystallized DRX grain size as obtained in hot compressions of a high-Mn steel.

The effect of temperature/strain rate on the DRX textures is illustrated in Figure 6, which shows the inverse pole figures for the compression axis direction. All compressed samples are characterized by similar textures irrespective of temperature and strain rate. Two texture fibers can be commonly distinguished in the inverse pole figures. Those are <001>||CA and <011>||CA. The latter one has been discussed as a preferred orientation for uniaxial compression of face-centered cubic (fcc) metals [27,28]. This fiber texture is the most pronounced in the partially recrystallized sample, which is characterized by the large work-hardened remnants of the original grains (Figure 6a). In contrast, the samples with fully DRX microstructures exhibit strong <001>||CA fiber textures. This fiber includes the Cube texture component, which has been considered as the preferred orientation for discontinuous recrystallization nucleation upon heating of cold rolled fcc-metal sheets [29,30]. Furthermore, Cube-oriented grains/subgrains are preferred to growth owing to their rapid dynamic recovery [29].

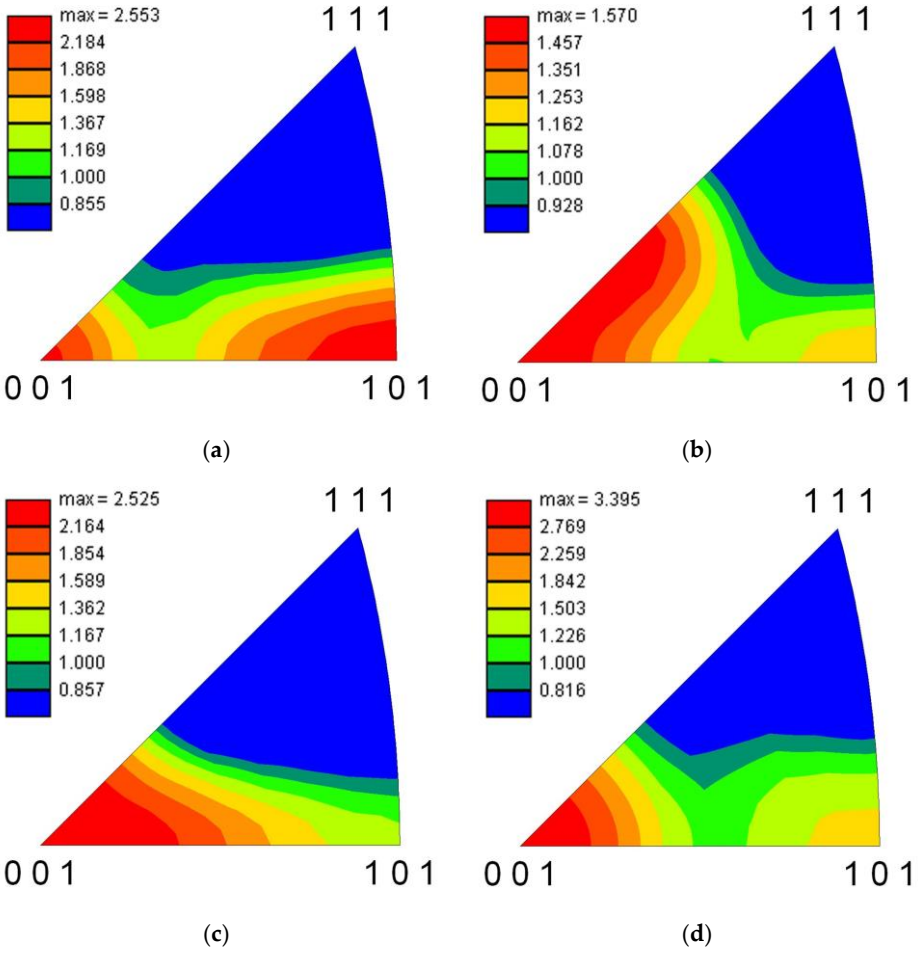

Figure 6. Inverse pole figures for a high-Mn steel subjected to hot compression at T = 1073 K and strain rate of 10^{-2} s^{-1} (**a**); at 1073 K and 10^{-3} s^{-1} (**b**); at 1223 K and 10^{-2} s^{-1} (**c**); and at 1323 K and 10^{-3} s^{-1} (**d**).

3.3. Tensile Tests

A series of the engineering stress-elongation curves after tensile tests of the steel samples processed by hot compression is shown in Figure 7, whereas strength and elongation are listed in Table 1. All samples demonstrate large elongations. It should be noted that uniform and total elongations are almost the same. This is typical tensile behavior of TWIP steels [12–14]. A decrease in the temperature and/or increase in the strain rate of the previous hot deformation results in significant strengthening. The yield strength and ultimate tensile strength are 305–540 MPa and 710–920 MPa, respectively,

depending on the hot working conditions. An increase in the strength is accompanied by a decrease in plasticity, although all samples with fully DRX microstructures exhibit total elongation well above 60%. Even the sample with the partially recrystallized necklace-type microstructure that evolved during compression at the highest temperature-compensated strain rate of about 10^{17} s^{-1} demonstrates uniform elongation above 50% along with a high yield strength of 540 MPa.

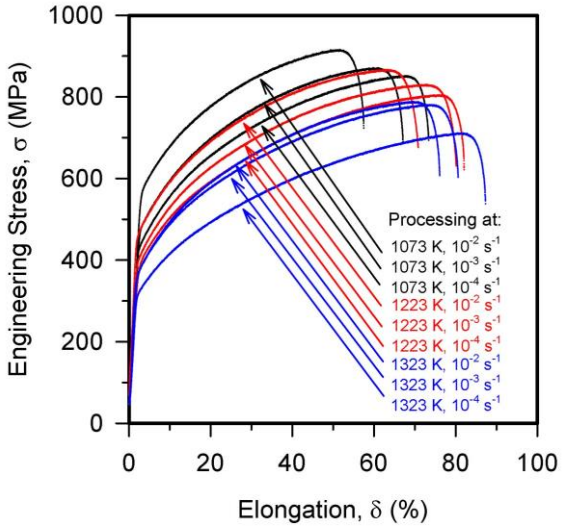

Figure 7. Engineering stress vs. elongation curves for a high-Mn steel subjected to hot compression at the indicated conditions.

Table 1. Some mechanical properties of a high-Mn steel processed by hot compression at the indicated temperatures and strain rates.

Temperature, K	Strain Rate, s^{-1}	Yield Strength, MPa	Ultimate Tensile Strength, MPa	Elongation, %
1073	10^{-2}	540	920	55
1073	10^{-3}	475	870	65
1073	10^{-4}	415	850	70
1223	10^{-2}	415	810	65
1223	10^{-3}	390	830	75
1223	10^{-4}	360	800	80
1323	10^{-2}	345	790	75
1323	10^{-3}	350	780	75
1323	10^{-4}	305	710	85

4. Discussion

4.1. DRX Mechanisms

The changes in the flow stress and DRX grain size dependence with a change in the deformation conditions in Figures 3 and 5 suggest that two DRX mechanisms operate in the present steel samples processed by warm-to-hot deformation. Discontinuous DRX develops during hot working under flow stress below approx. 100 MPa, whereas continuous DRX occurs under flow stresses above 100 MPa. The latter mechanism is associated with a gradual evolution of the strain-induced substructures, when the subgrain misorientations progressively increase up to the typical values of ordinary grain boundaries in a course of deformation [2].

Figure 8 represents enlarged Figure 4a,b images of the DRX microstructures evolved during the compressions under flow stresses of well above 100 MPa, corresponding to warm working conditions. Numerous incomplete grain boundaries, which terminate in grain interiors, can be seen in Figure 8 as shown by arrow heads. Such terminated grain boundaries are typical of a continuous DRX, when a portion of the deformation sub-boundary has its misorientation increased above a critical angle

($\theta \geq 15^\circ$ in the present study) and can be considered as a high-angle boundary while the rest of the sub-boundary is still in the range of low-angle misorientations [2,31]. On the other hand, numerous annealing twins (some of them are indicated by white lines in Figure 8) suggest frequent grain boundary migration, which is a typical feature of a discontinuous DRX [2,32,33]. Thus, the DRX microstructures evolved under warm working conditions result from the concurrent operation of both discontinuous and continuous DRX mechanisms. The change in the prevalent operating DRX mechanism from discontinuous to continuous with an increase in the temperature-compensated strain rate occurs gradually, i.e., their fractional contribution to the overall DRX changes in a rather wide range of deformation conditions. Slowing down the grain boundary mobility with a decrease in the deformation temperature suppresses the discontinuous DRX and, therefore, promotes a continuous DRX.

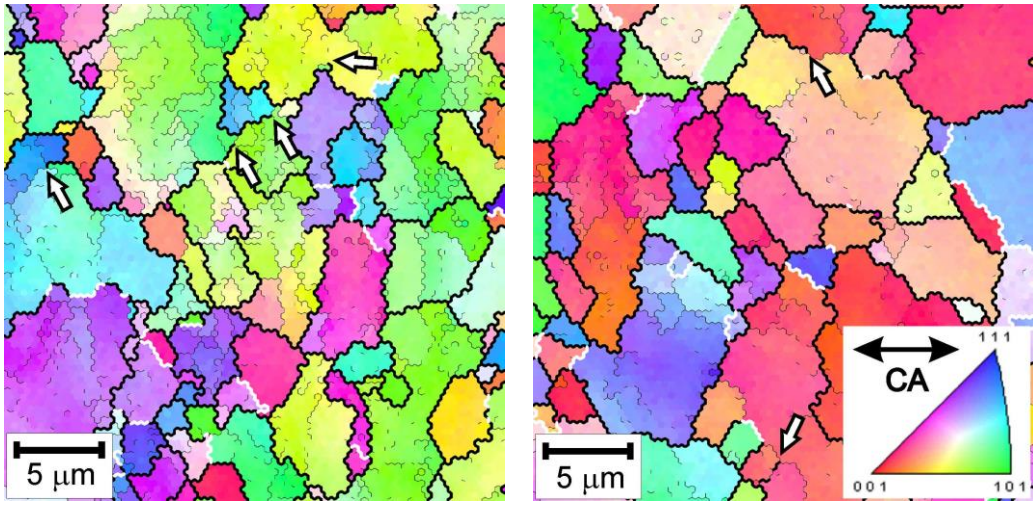

(**a**) (**b**)

Figure 8. The representative deformation microstructures evolved in a high-Mn steel during hot compression at a temperature of 1073 K and a strain rate of 10^{-2} s^{-1} (**a**) or 10^{-3} s^{-1} (**b**). The colors indicate the orientation along the compression axis (CA). The high-angle boundaries, low-angle sub-boundaries, and twin boundaries are shown by the thick black lines, thin black lines, and white lines, respectively.

The changes in the DRX textures are closely connected to the gradual change in the dominant DRX mechanism that is caused by a decrease in the grain boundary mobility as the deformation temperature decreases. Uniaxial compression of fcc-metals is commonly accompanied by an enhancement of <011>||CA fiber [27]. Then, the DRX grains with <001>||CA orientations nucleate during discontinuous recrystallization [30]. Following nucleation, the growth of DRX grains further increase the <001>||CA fiber [29]. Hence, the DRX microstructures developed under hot working conditions (low Z values) are characterized by a strong <001>||CA fiber, which weakens with increasing Z. At relatively low temperatures (high Z values), the limited growth of DRX nuclei weakens the <001>||CA fiber, while the compression-related <011>||CA fiber is enhanced.

The combined analysis of the deformation microstructures and textures reveals a very important feature of DRX during hot working of austenite. Namely, a remarkable portion of the DRX microstructures experiences large work-hardening irrespective of the prevailing DRX mechanism. The presence of work-hardened grains is expected in the case of a continuous DRX because the new grains are, essentially, the deformation subgrains, whose boundary misorientations exceed a critical value. Dynamic recovery, which assists continuous DRX, results in the dislocation rearrangement; however, progressive work-hardening takes place throughout the deformation. It is interesting that discontinuously recrystallized microstructures are also characterized by increased dislocation densities as proved by numerous low-angle sub-boundaries, which are clearly seen in Figures 4 and 8, and a high pole density for <110>||CA in Figure 6c,d. Therefore, the present DRX samples should

offer improved strength properties, which should be different from those in ordinary steels with annealed microstructures.

4.2. Strengthening by DRX

The strengthening due to the grain refinement is commonly discussed in terms of the Hall-Petch equation [34,35],

$$\sigma_{0.2} = \sigma_0 + k_y \cdot D^{-0.5} \quad (1)$$

Here, $\sigma_{0.2}$ is the yield strength, σ_0 is the Peierls stress, k_y is the grain boundary strengthening factor, and D is the mean grain size. The relationship between the DRX grain size and the yield strength of the present steel samples processed by hot compressions is shown in Figure 9. σ_0 = 210 MPa and k_y = 570 MPa $\mu m^{0.5}$ are obtained for the present steel samples. Figure 9 also shows the $\sigma_{0.2}$ vs. D relationship for a similar high-Mn steel subjected to primary static recrystallization (SRX) [36]. The value of σ_0 as obtained in the present study is quite close to that of 200 MPa, which has been reported for various austenitic stainless steels, although it is somewhat higher than that reported for a high-Mn steel with a SRX microstructure. It is worth noting that k_y in the present study is remarkably higher than that reported for the SRX steel. This can be attributed to an additional strengthening by the increased dislocation density in the DRX microstructures.

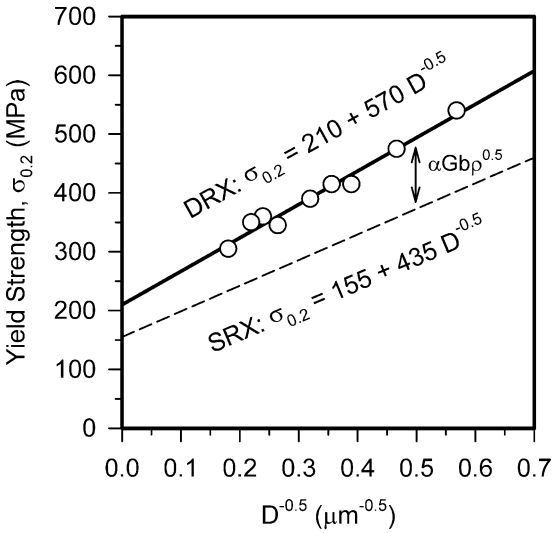

Figure 9. The effect of the DRX grain size on the yield strength of a high-Mn steel processed by hot compression.

The coarse remnants of the original grains contain a high density of low-angle dislocation sub-boundaries (Figure 8a). Thus, the partially recrystallized microstructure is characterized by the high dislocation density. Figure 4c,d suggests that other samples with microstructures, which were completely recrystallized during hot compression, also contain a relatively high dislocation density in the grain interiors as proved by numerous low-angle sub-boundaries. Therefore, the difference in the yield strength of the samples with statically and dynamically recrystallized microstructures can be expressed by a Tailor-type relationship [37],

$$\Delta\sigma_{0.2} = \alpha\, G\, b\, \rho^{0.5}, \quad (2)$$

where α is a numerical factor, G is the shear modulus, b is the Burgers vector, and ρ is the dislocation density. Assuming a linear function between the dislocation and grain size strengthenings [38–40] and taking α = 0.7 [41], G = 81,000 MPa, and b =2.6 × 10^{-10} m [20], the dislocation density in the present samples after hot compression can be evaluated varying from 3 × 10^{13} m^{-2} to 8 × 10^{13} m^{-2}. Note,

these values are close to those measured in an austenitic stainless steel after hot working under similar conditions [42]. It can be concluded, therefore, that DRX microstructures provide superior strength of high-Mn steels that can be expressed by unique Hall-Petch-type relationships irrespective of the combination of DRX mechanisms operating during hot working. In turn, hot working accompanied by DRX can be considered as a promising technology for the production of advanced high-Mn TWIP steels.

5. Conclusions

The hot deformation behavior, DRX microstructures, and the mechanical properties at ambient temperature of a high-Mn austenitic TWIP steel were studied. The main conclusions are listed below.

1. The flow stresses during hot deformation under hot working conditions with a temperature-compensated strain rate of $Z < 10^{14}$ s^{-1} exhibited strong temperature and strain rate dependencies and could be expressed by a power law function of Z with an exponent of about 0.2. In contrast, a much weaker temperature/strain rate dependency with an exponent of 0.1 was observed under conditions of $Z > 10^{15}$ s^{-1}.
2. Two DRX mechanisms, i.e., discontinuous and continuous ones, led to the new grain development, and their contribution depended on deformation conditions. Commonly, a power law function was obtained between the dynamic grain size and the steady-state flow stress. The discontinuous DRX resulted in a grain size exponent of -0.8 during deformation with the flow stresses below 100 MPa. This hot working domain corresponded to the temperature-compensated strain rate of $Z < 10^{14}$ s^{-1}. A decrease in deformation temperature and/or an increase in strain rate was accompanied by an increase in the contribution of the continuous DRX to the overall microstructure evolution under warm deformation conditions with the flow stress above 100 MPa ($Z > 10^{15}$ s^{-1}). Correspondingly, the grain size exponent in the power law function changed to about -0.5.
3. The grain refinement through DRX resulted in a remarkable strengthening of the present high-Mn steel. The ultimate tensile strength in the range of 700–900 MPa could be obtained. The yield strength could be expressed by a Hall-Petch-type equation with a rather high grain boundary strengthening factor of 570 MPa $\mu m^{0.5}$.

Author Contributions: Conceptualization, M.T. and A.B.; methodology, M.T. and A.B.; investigation, P.D.; writing—original draft preparation, A.B.; writing—review and editing, P.D. and R.K.; visualization, P.D.; supervision, R.K.

Funding: This research was funded by the Ministry of Science and Education of Russian Federation under the Grant No. 14.575.21.0134 (RFMEFI57517X0134).

Acknowledgments: Authors are grateful to the personnel of the Joint Research Center, Technology and Materials, Belgorod State University for their assistance with instrumental analysis.

Conflicts of Interest: The authors declare no conflict of interest.

References

1. McQueen, H.J.; Jonas, J.J. Recovery and Recrystallization during High Temperature Deformation. In *Treatise on Materials Science and Technology*; Arsenault, R.J., Ed.; Academic Press: New York, NY, USA, 1975; Volume 6, pp. 394–493.
2. Sakai, T.; Belyakov, A.; Kaibyshev, R.; Miura, H.; Jonas, J.J. Dynamic and post-dynamic recrystallization under hot, cold and severe plastic deformation conditions. *Prog. Mater. Sci.* **2014**, *60*, 130–207. [CrossRef]
3. Huang, K.; Loge, R.E. A review of dynamic recrystallization phenomena in metallic materials. *Mater. Des.* **2016**, *111*, 548–574. [CrossRef]
4. Luton, M.J.; Sellars, C.M. Dynamic recrystallization in nickel and nickel-iron alloys during high temperature deformation. *Acta Metall.* **1969**, *17*, 1033–1043. [CrossRef]
5. Jonas, J.J.; Sellars, C.M.; Tegart, W.J.M. Strength and structure under hot-working conditions. *Metall. Rev.* **1969**, *14*, 1–24.

6. Sakai, T.; Jonas, J.J. Dynamic recrystallization: Mechanical and microstructural considerations. *Acta Metall.* **1984**, *32*, 189–209. [CrossRef]
7. Sakai, T. Dynamic recrystallization microstrustures under hot working conditions. *J. Mater. Process. Technol.* **1995**, *53*, 349–361. [CrossRef]
8. Poliak, E.I.; Jonas, J.J. A one-parameter approach to determining the critical conditions for the initiation of dynamic recrystallization. *Acta Metall. Mater.* **1996**, *44*, 127–136. [CrossRef]
9. Jonas, J.J.; Quelennec, X.; Jiang, L.; Martin, E. The Avrami kinetics of dynamic recrystallization. *Acta Mater.* **2009**, *57*, 2748–2756. [CrossRef]
10. Chen, M.-S.; Lin, Y.C.; Ma, X.-S. The kinetics of dynamic recrystallization of 42CrMo steel. *Mater. Sci. Eng. A* **2012**, *A556*, 260–266. [CrossRef]
11. Yanushkevich, Z.; Belyakov, A.; Kaibyshev, R. Microstructural evolution of a 304-type austenitic stainless steel during rolling at temperatures of 773–1273 K. *Acta Mater.* **2015**, *82*, 244–254. [CrossRef]
12. Bouaziz, O.; Allain, S.; Scott, C.P.; Cugy, P.; Barbier, D. High manganese austenitic twinning induced plasticity steels: A review of the microstructure properties relationships. *Curr. Opin. Solid State Mater. Sci.* **2011**, *15*, 141–168. [CrossRef]
13. Kusakin, P.S.; Kaibyshev, R.O. High-Mn twinning-induced plasticity steels: Microstructure and mechanical properties. *Rev. Adv. Mater. Sci.* **2016**, *44*, 326–360.
14. De Cooman, B.C.; Estrin, Y.; Kim, S.K. Twinning-induced plasticity (TWIP) steels. *Acta Mater.* **2018**, *142*, 283–362. [CrossRef]
15. Grässel, O.; Krüger, L.; Frommeyer, G.; Meyer, L.W. High strength Fe-Mn-(Al, Si) TRIP/TWIP steels development-Properties-Application. *Int. J. Plast.* **2000**, *16*, 1391–1409. [CrossRef]
16. Ryan, N.D.; McQueen, H.J. Dynamic softening mechanisms in 304 austenitic stainless steel. *Can. Metall. Q.* **1990**, *29*, 147–162. [CrossRef]
17. Belyakov, A.; Miura, H.; Sakai, T. Dynamic recrystallization under warm deformation of a 304 type austenitic stainless steel. *Mater. Sci. Eng. A* **1998**, *A255*, 139–147. [CrossRef]
18. Tikhonova, M.; Kaibyshev, R.; Belyakov, A. Microstructure and mechanical properties of austenitic stainless steels after dynamic and post-dynamic recrystallization treatment. *Adv. Eng. Mater.* **2018**, *20*, 1700960. [CrossRef]
19. Derby, B. The dependence of grain size on stress during dynamic recrystallization. *Acta Metall. Mater.* **1991**, *39*, 955–962. [CrossRef]
20. Frost, H.J.; Ashby, M.F. *Deformation Mechanism Maps*; Pergamon Press: Oxford, UK, 1982.
21. Maki, T.; Akasaka, K.; Okuno, K.; Tamura, I. Dynamic recrystallization of austenite in 18-8 stainless steel and 18 Ni maraging steel. *Trans. ISIJ* **1982**, *22*, 253–261. [CrossRef]
22. Humphreys, F.J.; Hatherly, M. *Recrystallization and Related Annealing Phenomena*; Elsevier Science: New York, NY, USA, 2004.
23. Liu, Y.-X.; Lin, Y.C.; Zhou, Y. A 2D cellular automaton simulation of hot deformation behavior in a Ni-based superalloy under varying thermal-mechanical conditions. *Mater. Sci. Eng. A* **2017**, *A691*, 88–99. [CrossRef]
24. Sherby, O.D.; Burke, P.M. Mechanical behavior of crystalline solids at elevated temperature. *Prog. Mater. Sci.* **1967**, *13*, 325–390. [CrossRef]
25. Dudova, N.; Belyakov, A.; Sakai, T.; Kaibyshev, R. Dynamic recrystallization mechanisms operating in a Ni-20%Cr alloy under hot-to-warm working. *Acta Mater.* **2010**, *58*, 3624–3632. [CrossRef]
26. Tikhonova, M.; Belyakov, A.; Kaibyshev, R. Strain-induced grain evolution in an austenitic stainless steel under warm multiple forging. *Mater. Sci. Eng. A* **2013**, *A564*, 413–422. [CrossRef]
27. Bishop, J.F.W. A theory of the tensile and compressive textures of face-centred cubic metals. *J. Mech. Phys. Solids* **1955**, *3*, 130–142. [CrossRef]
28. Gil Sevillano, J.; van Houtte, P.; Aernoudt, E. Large strain work hardening and textures. *Prog. Mater. Sci.* **1980**, *25*, 69–134. [CrossRef]
29. Hutchinson, B.; Nes, E. Texture development during grain growth—A useful rule-of-thumb. *Mater. Sci. Forum.* **1992**, *94–96*, 385–390. [CrossRef]
30. Engler, O.; Vatne, H.E.; Nes, E. The roles of oriented nucleation and oriented growth on recrystallization textures in commercial purity aluminium. *Mater. Sci. Eng. A* **1996**, *A205*, 187–198. [CrossRef]
31. Cizek, P. The microstructure evolution and softening processes during high-temperature deformation of a 21Cr-10Ni-3Mo duplex stainless steel. *Acta Mater.* **2016**, *106*, 129–143. [CrossRef]

32. Tikhonova, M.; Dolzhenko, P.; Kaibyshev, R.; Belyakov, A. Grain boundary assemblies in dynamically-recrystallized austenitic stainless steel. *Metals* **2016**, *6*, 268. [CrossRef]
33. He, D.-G.; Lin, Y.C.; Huang, J.; Tang, Y. EBSD Study of Microstructural Evolution in a Nickel-Base Superalloy during Two-Pass Hot Compressive Deformation. *Adv. Eng. Mater.* **2018**, *20*, 1800129. [CrossRef]
34. Hall, E.O. The deformation and ageing of mild steel: III discussion of results. *Proc. R. Soc. Lond. Ser. B* **1951**, *64*, 747–753. [CrossRef]
35. Petch, N.J. The cleavage strength of polycrystals. *J. Iron Steel Inst.* **1953**, *174*, 25–28.
36. Yanushkevich, Z.; Belyakov, A.; Kaibyshev, R.; Haase, C.; Molodov, D.A. Effect of cold rolling on recrystallization and tensile behavior of a high-Mn steel. *Mater. Charact.* **2016**, *112*, 180–187. [CrossRef]
37. Estrin, Y.; Toth, L.S.; Molinari, A.; Brechet, Y. A dislocation-based model for all hardening stages in large strain deformation. *Acta Mater.* **1998**, *46*, 5509–5522. [CrossRef]
38. Shakhova, I.; Belyakov, A.; Yanushkevich, Z.; Tsuzaki, K.; Kaibyshev, R. On strengthening of austenitic stainless steel by large strain cold working. *ISIJ Int.* **2016**, *56*, 1289–1296. [CrossRef]
39. Starink, M.J. Dislocation versus grain boundary strengthening in SPD processed metals: Non-causal relation between grain size and strength of deformed polycrystals. *Mater. Sci. Eng. A* **2017**, *A705*, 42–45. [CrossRef]
40. Yanushkevich, Z.; Dobatkin, S.V.; Belyakov, A.; Kaibyshev, R. Hall–Petch relationship for austenitic stainless steels processed by large strain warm rolling. *Acta Mater.* **2017**, *136*, 39–48. [CrossRef]
41. Ma, K.; Smith, T.; Hu, T.; Topping, T.D.; Lavernia, E.J.; Schoenung, J.M. Distinct hardening behavior of ultrafine-grained Al-Zn-Mg-Cu alloy. *Metall. Mater. Trans. A* **2014**, *45*, 4762–4765. [CrossRef]
42. Belyakov, A.; Sakai, T.; Miura, H.; Kaibyshev, R. Grain refinement under multiple warm deformation in 304 type austenitic stainless steel. *ISIJ Int.* **1999**, *39*, 592–599. [CrossRef]